

## Interplay of Rabi Oscillations and Quantum Interference in Semiconductor Quantum Dots

H. Htoon,<sup>1</sup> T. Takagahara,<sup>2</sup> D. Kulik,<sup>1</sup> O. Baklenov,<sup>3</sup> A. L. Holmes, Jr.,<sup>3,4</sup> and C. K. Shih<sup>1,4</sup>

<sup>1</sup>*Department of Physics, University of Texas at Austin, Austin, Texas 78712*

<sup>2</sup>*Department of Electronics and Information Science, Kyoto Institute of Technology, Kyoto 606-8585, Japan*

<sup>3</sup>*Department of Electrical and Computer Engineering, University of Texas at Austin, Austin, Texas 78712*

<sup>4</sup>*Texas Materials Institute, University of Texas at Austin, Austin, Texas 78712*

(Received 9 October 2001; published 7 February 2002)

We investigated the manifestation of Rabi oscillation in the coherent dynamics of excitons in self-assembled semiconductor quantum dots. The Rabi oscillation phenomenon was directly observed as a function of the input pulse area. Furthermore, by performing wave packet interferometry in the nonlinear excitation regime, we discover a new type of quantum interference phenomenon, resulting from the interplay between Rabi oscillation and quantum interference.

DOI: 10.1103/PhysRevLett.88.087401

PACS numbers: 78.67.Hc, 42.50.Hz, 78.47.+p, 78.55.-m

Coherent manipulation of quantum states is a critical step toward many novel technological applications ranging from manipulation of “qubits” in quantum logic gates [1] to controlling the reaction pathways of molecules [2]. Both Rabi oscillation (RO) and quantum interference (QI) play central roles in coherent control. In the strong excitation regime, RO provides a direct control to the excited state population of a quantum system through the input area (i.e., time integrated Rabi frequency) of a single excitation pulse [3]. On the other hand, in the weak excitation regime, the quantum interference of probability waves excited with phase-tailored pulse pairs is utilized for wave function manipulation in atoms [4], molecules [2], and semiconductor heterostructures [5].

Atomlike states of semiconductor quantum dots (SQDs) have been envisioned to be the building blocks of the solid-state quantum computer [1]. This technological motivation intensifies research efforts in coherent phenomena of SQDs. Numerous fundamental coherent properties common to ideal quantum systems such as atomic-like spectra [6,7], entanglement [8], photon antibunching [9], the modification of spontaneous emission rate by a microcavity [10], and coherent wave function manipulation by using QI [7,11] have been recently demonstrated in various types of SQDs. However, there have been very few investigations on RO in SQDs [12,13]. This fundamental coherent phenomenon stands as a principal criterion in establishing an analogy among the fundamentally different quantum states of atomic/molecular systems [14–16] and semiconductors [17,18]. Furthermore, a recent theoretical investigation by one of the authors [13] predicted a dramatic change of quantum interference patterns when the excitation strengths of the phase-tailored pulse pairs become strong enough to induce nonlinear effects of RO in an excited state population. This new quantum interference phenomenon leads to the possibility of combining RO and QI to provide a new scenario of coherent manipulation.

In this Letter, we present *direct experimental evidence of Rabi oscillation* in individual self-assembled quantum dots

(SAQDs). This study not only demonstrates a fundamental optical effect but also provides a way to determine optical properties such as dipole moments and radiative lifetimes. Furthermore, we report on the experimental observation of *the new quantum interference phenomenon* described above. In addition, our detailed theoretical investigations attribute this phenomenon to the interplay between RO and QI. Although RO has been recently observed in a differential transmission study of SQDs [12], the time domain coherent dynamics of this phenomenon are totally unexplored. The evolution of our new QI patterns with relative phase and energy detuning of the pulse pairs reveals these coherent dynamics effects.

Our QD sample is a six-monolayer-thick  $\text{In}_{0.5}\text{Ga}_{0.5}\text{As}$  SAQD grown by molecular beam epitaxy [19]. Cross-sectional scanning tunneling microscopy studies revealed that the QDs have average height, lateral dimensions, and dot-to-dot separation of 4.5, 20–40, and 100 nm, respectively. We used a mode locked Ti:sapphire laser ( $\Delta t_{\text{FWHM}} \sim 6$  ps and repetition rate of 82 MHz). We performed resonant excitation and collection of the photoluminescence (PL) signal on the cleaved edge of the sample to reduce the number of probed QDs effectively. The PL signals of QDs locating along the cleaved edge are dispersed by using the spectrograph and then imaged individually onto the array detector. (See Ref. [20] for further details of single dot spectroscopy.) All of our measurements were done at 15 K. We have conducted extensive investigations on energy level structures and dephasing processes of the excited states of this particular QD sample [7]. These studies revealed that the first excited states of some of the QDs are energetically isolated from other states and have very long dephasing times ( $T_2$ 's) of 40–90 ps [7]. Since these two are important criteria for the observation of RO, we concentrated our studies on this kind of excited state.

It has been well known that the population of the excited state under strong resonant excitation undergoes a sinusoidal oscillation (RO) as the function of input pulse area  $\theta$  defined by  $\theta(t) = \int_{-\infty}^t \frac{\mu}{\hbar} \varepsilon(t') dt'$ , where  $\varepsilon(t)$  and

$\mu$  are the envelope function of the laser pulses and the transition dipole moment of a two-level system, respectively [3]. In atomic and molecular systems, this phenomenon had been directly observed by measuring the fluorescence signal as the function of input pulse area [15]. We report a similar experiment on an excited state of an individual SAQD. We can consider the SAQD as a three-level system shown in the inset of Fig. 1(a). We resonantly excited the  $|2\rangle$  state. Since this state is nonradiatively coupled to the exciton ground state ( $|3\rangle$ ), the population of the  $|2\rangle$  state can be monitored through the PL intensity of the  $|3\rangle$  state. Figure 1(a) displays the PL intensity as the function of the square root of the average power density, which is directly proportional to the total input area of our mode locked laser pulse. The plot clearly shows the oscillation very similar to those shown in Ref. [15]. This is the direct observation of Rabi oscillation in an excited state of a SAQD. A portion of the excited state population loses its phase coherence during the pulse excitation. While this portion can no longer participate in RO, it still contributes to the PL signal of the  $|3\rangle$  state and gives rise to the residual signal observed at  $2\pi$  excitation.

This simple experiment also provides an effective way of measuring several important optical properties. For example, the input area  $\theta$  of the pulse can be determined by assigning the excitation strength at the maximum/minimum points of Fig. 1(a) to  $\theta$  values of integral multiples of  $\pi$ . The determined values are given on the bottom axis. Furthermore, the transition dipole moment  $\mu$  can be calculated from these estimated  $\theta$ 's. The dipole moment of this particular QD is 20 D. The  $\mu$ 's of the QDs we measured are in the range from 9.0 to 40 D.

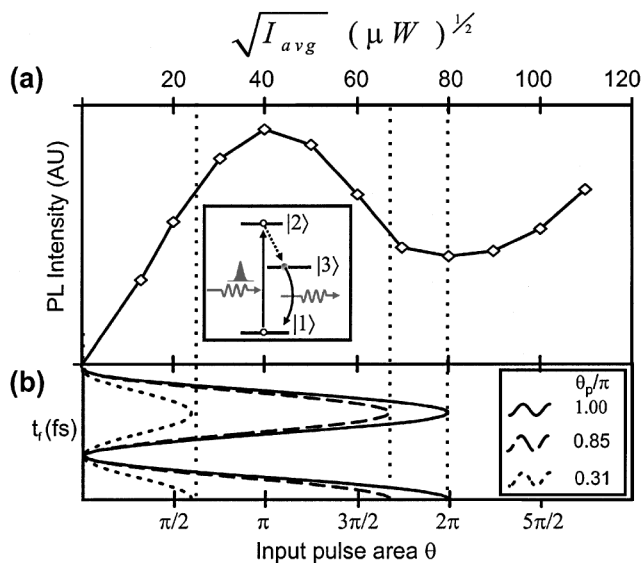


FIG. 1. (a) The plot of PL intensity of state  $|3\rangle$  vs the square root of average excitation intensity showing the Rabi oscillation. Inset: Schematic of interaction. (b) Modulation of  $\theta$  as the function of  $t_f$  at  $t_d = 0$  ps (see Fig. 2).

To study the coherent dynamics resulting from the interplay of RO and QI, we performed the single dot wave packet interferometry measurements in the strong excitation regime. In similar studies conducted at the weak excitation regime [7,11], the QI generated by the resonant excitations with picosecond pulse pairs [Fig. 2(a)] gives rise to the sinusoidal oscillation of an excited states population as the function of time delay. This oscillation (at optical frequency) was monitored through PL of the  $|3\rangle$  state [inset of Fig. 2(b)]. The envelopes of the oscillations undergo symmetric exponential decay due to dephasing [Fig. 2(b)]. These two key features of QI, sinusoidal oscillation at the fine time scale and symmetric exponential decay of the envelopes at the long time scale, change dramatically in the strong excitation regime.

Figure 2(c) shows the fine time ( $t_f$ ) scale QI patterns measured at different coarse time delay steps ( $t_d$ 's) and excitation strengths. The excitation strength is given in terms of the input area per pulse ( $\theta_p$ ) of the excitation pulse pairs. For all the steps of  $t_d$ 's, the oscillation of the excited state population with  $t_f$  is sinusoidal at weak excitations (i.e.,  $\theta_p < 0.3\pi$ ). At strong excitations, while patterns observed at  $t_d$  longer than 16 ps are nearly sinusoidal, the oscillation patterns become nonsinusoidal for  $t_d$ 's less than 16 ps [Fig. 2(c)]. Furthermore, these patterns change as we detuned the excitation energy away from the resonance, as shown in Fig. 3(a). At  $t_d = 0$  ps, all the patterns show a doublet peak at the maximums of fine time scale

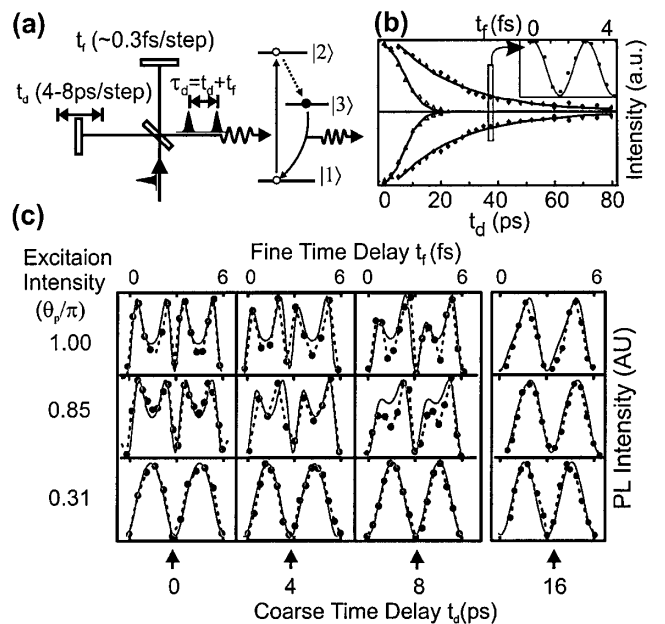


FIG. 2. (a) Schematic of the interaction. (b) QI patterns at weak excitation shown together with the autocorrelation of pulse pairs. (c) Fine time scale oscillation patterns at different coarse time delay steps and excitation strengths. Data points connected by dashed lines: Experimental data. Gray solid lines: Theoretical calculations. Signals are normalized for clarity.

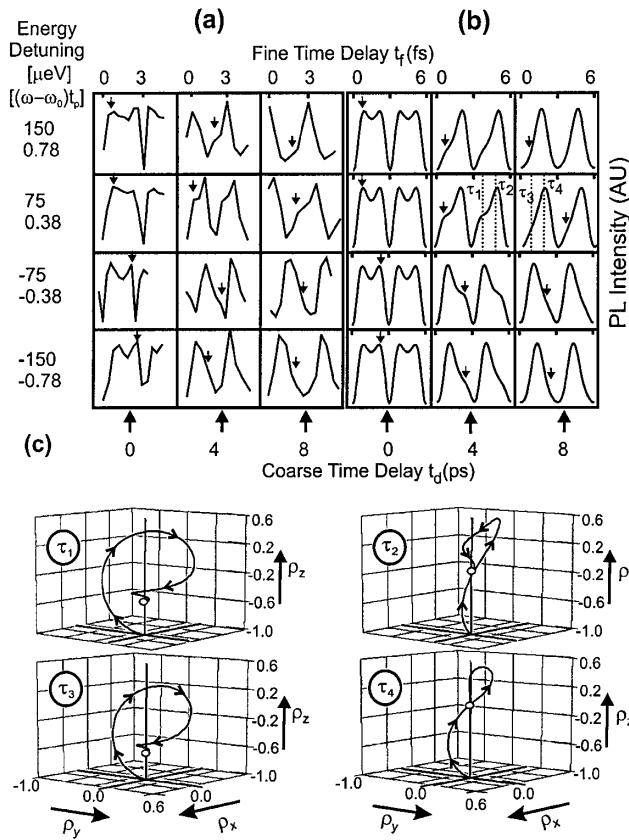


FIG. 3. (a) Detuning dependence of nonsinusoidal oscillation patterns at  $\theta_p/\pi = 0.75$ . Experimental. (b) Theoretical results. (c) Trajectories of the Bloch vector traced during the excitation period for time delays  $\tau_1 - \tau_4$  indicated in the second row of (b) where  $\tau_1, \tau_2, \tau_3,$  and  $\tau_4$  are 4004, 4005.1, 8000.8, and 8001.9 fs, respectively.

modulations. When the detuning is positive, the left peak of the doublet drops down as  $t_d$  increases. (See the indicator arrows.) The right peak drops with the increase of  $t_d$  for negative detuning.

The qualitative understanding can be attained by analyzing the effect of modulation in the total input area of the pulse pairs ( $\theta_{\text{total}}$ ). When two pulses of the excitation pairs are completely overlapped at  $t_d = 0$  ps, scanning  $t_f$  with fine steps, as shown in Fig. 2(a), simply modulates the electric field and  $\theta_{\text{total}}$  via the optical interference. Figure 1(b) shows this oscillation of  $\theta_{\text{total}}$  for three excitation strengths of Fig. 2(c). At low excitation strengths of  $\theta_p \leq 0.3\pi$ , the approximately linear dependence of excited state population upon  $\theta_{\text{total}}$  leads to the simple sinusoidal oscillation of the population as the function of  $t_f$ . As  $\theta_{\text{total}}$  increases beyond  $\pi$ , the population at the maximum pulse area decreases due to RO and the dip at the peak of sinusoidal oscillation appears as shown in Fig. 2(c). This dip goes deeper as the maximum of  $\theta_{\text{total}}$  approaches  $2\pi$ . At  $\theta_{\text{total}} = 2\pi$ , the dip would reach to the bottom if there were no dephasing. However, dephasing of some population during the pulse excitation gives a residual PL signal

as discussed earlier. At  $t_d$ 's longer than 16 ps (i.e.,  $\sim 2\Delta t$ ),  $\theta_{\text{total}}$  no longer varies with  $t_f$ . Therefore, the interference of two wave packets with phase difference  $\omega\tau_d$  leads to the sinusoidal oscillation for all the excitation strengths.

To gain quantitative understanding on the details of these patterns, we performed density matrix calculations, taking the experimentally determined  $\theta_p$  (from Fig. 1) and dephasing time ( $T_2$ ) as input parameters. We consider the interaction between the three-level system shown in Fig. 2(a) and the excitation laser pulse pairs with the electric field of  $E(t) = \varepsilon(t) \cos(\omega t) + \varepsilon(t - \tau_d) \cos[\omega(t - \tau_d)]$ , where  $\varepsilon(t) = \varepsilon_0 \text{sech}(t/t_p)$ . For the initial state of our experiment, i.e.,  $\rho_{11}(t=0) = 1$  and other  $\rho_{ij}(t=0) = 0$ , only  $\rho_{11}, \rho_{22}, \rho_{33}, \rho_{21},$  and  $\rho_{12}$  components of the density matrix are to be included in the calculations since the coherences of  $\rho_{13}$  and  $\rho_{23}$  are not induced. Our signal is proportional to  $\int_0^\infty \rho_{33}(t) dt$ , which is, in turn, proportional to  $\int_0^\infty \rho_{22}(t) dt$ .  $\rho_{22}(t)$  in the long time region can further be expressed as  $\rho_{22}(t) = \rho_{22}^0 e^{-\gamma t}$ , where  $\gamma$  and  $\rho_{22}^0$  are the population decay rate and the value of  $\rho_{22}$  just after the pulse pair, respectively. Results of full numerical calculations are shown in Figs. 2(c) (gray solid lines) and 3(b). The theoretical simulation well reproduces the main features of nonsinusoidal oscillation patterns as well as the trends in their variations with excitation strength, delay time, and energy detuning.

The coherent dynamical processes can be conceptually visualized as the motion of the Bloch vector  $\vec{\rho}$  whose  $z$  component represents the population inversion ( $\rho_z = \rho_{22} - \rho_{11}$ ) [3]. The motion can be described by the Bloch model  $\dot{\vec{\rho}} = \vec{\rho} \times \vec{G} - \Gamma \vec{\rho}$  with the gyration vector,

$$\vec{G} = \begin{pmatrix} \Omega_0 \{ \text{sech}(t/t_p) + \text{sech}[(t - \tau_d)/t_p] \cos(\omega\tau_d) \} \\ \Omega_0 \text{sech}[(t - \tau_d)/t_p] \sin(\omega\tau_d) \\ \Delta\omega \end{pmatrix}.$$

where  $\Omega_0, \tau_d, \Delta\omega,$  and  $\Gamma \vec{\rho}$  denote the Rabi frequency ( $\mu\varepsilon_0/\hbar$ ), the total time delay ( $t_d + t_f$ ), the amount of detuning from the resonance, and the relaxation terms, respectively. Excitation with pulse pairs gives the phase factors  $\cos(\omega\tau_d)$  and  $\sin(\omega\tau_d)$ . Because of these phase factors, the trajectories of  $\vec{\rho}$ 's traced during the excitation become strongly dependent upon  $\tau_d$ . The trajectories calculated for four different  $\tau_d$ 's, ( $\tau_1 - \tau_4$ ) [see second row of Fig. 3(b)], are shown in Fig. 3(c) as examples. The last points of the traces, indicated by white circles, reflect the values of  $\rho_{22}^0$ 's. At  $\tau_1$  and  $\tau_3$ , the  $\vec{\rho}$ 's start from the south pole of the Bloch sphere and turn around to the vicinity of the south pole, leading to low signals. On the other hand, at  $\tau_2$  and  $\tau_4$ , the  $\vec{\rho}$ 's do not return to the neighborhood of the south pole, and  $\rho_{22}^0$ 's retain large values. These inspections provide understanding on how the interplay of RO and QI drives the  $\vec{\rho}$  and gives rise to the  $t_f$  scale oscillation patterns.

In addition to the fine time scale oscillation features, the decay of the envelopes at a long time scale also changes dramatically. In Fig. 4(a), we plotted the envelopes of the

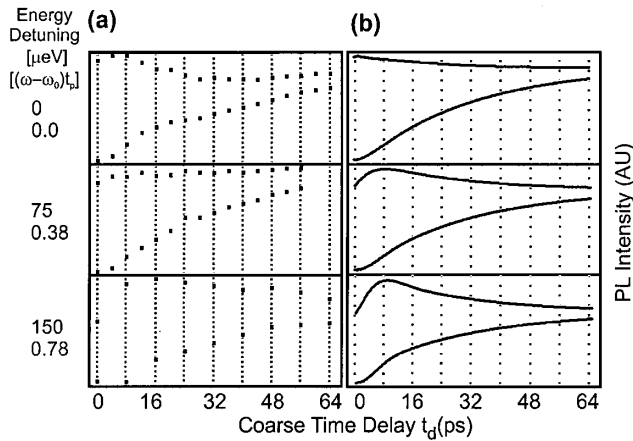


FIG. 4. Evolution of oscillation envelopes with the energy detuning at  $\theta_p/\pi = 0.6$ ; (a) experimental; (b) theoretical.

fine time scale oscillations as a function of  $t_d$  and  $\Delta\omega$ . All the figures clearly show that the envelopes of maximums and minimums are no longer symmetric as in the low excitation strength case [Fig. 2(b)]. The results of the calculations [Fig. 4(b)] also show similar asymmetric decays in agreement with the experiment. In the linear (weak excitation) regime, the pulse pairs induce the constructive and destructive quantum interference of carrier waves, and the correlation trace shows a symmetric decay pattern toward the long  $t_d$ 's where two pulses contribute independently to the signal. On the other hand, in the nonlinear (strong excitation) regime, the population of the exciton ground state  $|3\rangle$  accumulates during the pulse interval and pushes up the minimum envelope of the correlation trace, leading to the observed asymmetric decay.

At a low excitation strength, the envelope of maximums always has its peak at  $t_d = 0$  ps, irrespective of detuning from the resonance ( $\Delta\omega$ ). However, in the strong excitation regime, a dip in the envelope of maximums appears at  $\Delta\omega \neq 0$ , and it goes deeper and wider as  $\Delta\omega$  increases [Fig. 4(a)]. This “dip feature,” also reproduced in the calculations [Fig. 4(b)], can be explained by using the Bloch vector model. In the presence of  $\Delta\omega$ , the gyration vector  $\vec{G}$  deviates from the horizontal plane, and the complete overlap of two pulses at  $t_d = 0$  ps does not always yield the maximum value of  $\rho_{22}$ . Instead, some values of  $t_d$ 's are more effective to push up the Bloch vector leading to a large value of  $\rho_{22}$ . This is again a consequence of the sensitive dependence of the  $\vec{G}$  on  $\tau_d$ .

In summary, we explored the manifestation of Rabi oscillation in the coherent dynamics of excitons in SAQDs. Rabi oscillation was directly observed. In addition, experimental and theoretical investigations revealed that the interplay between RO and QI gives rise to a new type of quantum interference phenomenon. This phenomenon

could be utilized to manipulate the amplitude and the phase of the probability waves simultaneously, thus providing a possible new scenario of coherent manipulation.

This work was supported by NSF-DMR 0071893, NSF Science and Technology Center, Grant No. CHE 8920120, and the W.M. Keck Foundation. The computation in this work has been done using the facilities of Supercomputer Center, Institute for Solid State Physics, University of Tokyo, Japan.

- [1] C. H. Bennett and D. P. DiVincenzo, *Nature (London)* **404**, 247 (2000); A. Barenco *et al.*, *Phys. Rev. Lett.* **74**, 4083 (1995); P. Chen *et al.*, *ibid.* **87**, 067401 (2001); E. Biolatti *et al.*, *ibid.* **85**, 5647 (2000); F. Troiani *et al.*, *Phys. Rev. B* **62**, 2263(R) (2000).
- [2] R. N. Zare, *Science* **279**, 1875 (1998), and references therein.
- [3] L. Allen and J. H. Eberly, *Optical Resonance and Two Level Atoms* (Wiley, New York, 1975).
- [4] D. M. Meekhof *et al.*, *Phys. Rev. Lett.* **76**, 1796 (1996); J. A. Yeazell and C. R. Stroud, Jr., *ibid.* **60**, 1494 (1988).
- [5] A. P. Heberle, J. J. Baumberg, and K. Kohler, *Phys. Rev. Lett.* **75**, 2598 (1995); X. Marie *et al.*, *ibid.* **79**, 3222 (1997).
- [6] D. Gammon *et al.*, *Science* **273**, 87 (1997); K. Brunner *et al.*, *Phys. Rev. Lett.* **73**, 1138 (1994); P. Hawrylak *et al.*, *ibid.* **85**, 389 (2000); M. Bayer *et al.*, *Nature (London)* **405**, 923 (2000).
- [7] H. Htoon *et al.*, *Phys. Rev. B* **63**, 241303(R) (2001).
- [8] G. Chen *et al.*, *Science* **289**, 1906 (2000); M. Bayer *et al.*, *ibid.* **291**, 451 (2001).
- [9] C. Becher *et al.*, *Phys. Rev. B* **63**, 121312(R) (2001); P. Michler *et al.*, *Nature (London)* **406**, 968 (2000).
- [10] G. S. Solomon, M. Pelton, and Y. Yamamoto, *Phys. Rev. Lett.* **86**, 3903 (2001).
- [11] N. H. Bonadeo *et al.*, *Science* **282**, 1473 (1998); Y. Toda *et al.*, *Appl. Phys. Lett.* **76**, 3887 (2000).
- [12] T. H. Stievater *et al.*, *Phys. Rev. Lett.* **87**, 133603 (2001).
- [13] T. Takagahara, *Technical Digest of QELS 2001* (OSA, Washington, DC, 2001), Vol. 57, p. 19.
- [14] I. I. Rabi, *Phys. Rev.* **51**, 652 (1937); I. I. Rabi *et al.*, *ibid.* **55**, 626 (1939); H. C. Torrey, *ibid.* **76**, 1059 (1949).
- [15] H. M. Gibbs, *Phys. Rev. A* **8**, 446 (1973); Y. S. Bai, A. G. Yodh, and T. W. Mossberg, *Phys. Rev. Lett.* **55**, 1277 (1985).
- [16] G. B. Hocker and C. L. Tang, *Phys. Rev. Lett.* **21**, 591 (1968); P. W. Hoff, H. A. Haus, and T. J. Bridges, *ibid.* **25**, 82 (1970).
- [17] B. E. Cole *et al.*, *Nature (London)* **410**, 60 (2001).
- [18] A. Schülzgen *et al.*, *Phys. Rev. Lett.* **82**, 2346 (1999); S. T. Cundiff *et al.*, *ibid.* **73**, 1178 (1994); J. Devis, E. Diez, and V. Bellani, *Phys. Lett. A* **255**, 349 (1999).
- [19] O. Baklenov *et al.*, *J. Vac. Sci. Technol. B* **17**, 1124 (1999).
- [20] H. Htoon *et al.*, *Appl. Phys. Lett.* **76**, 700 (2000); *Phys. Rev. B* **60**, 11 026 (1999).